Discrete element modeling of a trafficked sub-base stabilized with biaxial and multi-axial geogrids to compare stabilization mechanisms

H. Jas, 7asConsult BV, Oostvoorne, The Netherlands, hein@7asconsult.nl
M. Stahl, Schüßler-Plan Ingenieurgesellschaft mbH, Düsseldorf, Germany, MStahl@schuessler-plan.de
H. Konietzky, Geotechnical Institute, TU Bergakademie Freiberg, Germany, heinz.konietzky@ifgt.tu-freiberg.de
L. te Kamp, ITASCA Consultants GmbH, Gelsenkirchen, Germany, Ltekamp@itasca.de
T. Oliver, Tensar International, Blackburn, UK, toliver@tensar.co.uk

ABSTRACT
A particle-based three dimensional numerical simulation is presented for the generation of geogrid-stabilized sub-base over a weak soil while trafficked. The paper describes how a section of unpaved sub-base is modelled, describing the calibration conditions of the components as well as some specific model conditions. Model analyses of 10 runs of a wheel driving over the sub-base stabilized with a biaxial geogrid with square apertures and hexagonal TX (multi-axial) geogrid with triangular apertures are presented to better understand the significant properties of the geogrids for the function of stabilization. These analyses include the specific movements of the granular particles of the sub-base, the movements of the geogrids as well as the generated stresses and strains in the ribs and junctions of the geogrid in three dimensions. The results of the analyses indicate a clear difference in stabilization mechanism between the two types of geogrid.

1. INTRODUCTION

In the fields of ground and road engineering, the use and acceptance of geogrids has increased over the past 30 years. The stiff ribs and junctions of punched and stretched geogrids allow the soil particles to penetrate into the apertures during the compaction process (interlocking), whereby the particles are confined within the boundaries of the apertures. In practice, several design methods with geogrids are in use, but most of them are empirical and none incorporate the interaction between soil and geogrid at the micro-level, as this mechanism is not yet well understood.

The three dimensional discrete element method-based Particle Flow Code PFC_{3D} simulates the mechanical behavior of a system comprised of rigid spherical particles and wall elements. This method offers good chances to model the behavior of the soil–geogrid interaction in a realistic manner. For this purpose, a realistic soil model is required in which the simulated grains have the ability to penetrate into the apertures of a geogrid model in a proper manner. A particle-based numerical simulation procedure in PFC_{3D} was presented by Stahl and Konietzky (2011), which allows the modelling of stiff granular material (ballast or gravel) using the clump logic under special consideration of grain shape, grain size and relative density. This code allows a much more realistic simulation than the highly simplified two-dimensional approach which is used by for instance Ziegler et all (2008).

This paper describes how (granular) soils and geogrids are simulated depending on a specific particle and parallel bond model and calibrated to laboratory tests conducted on real soils. Numerical and experimental pull-out tests have been performed to reproduce the behavior of geogrid specimens embedded in granular material under special consideration of the grain-size distribution, initial relative density, normal stress state as well as sample installation (Stahl and Konietzky 2011). True calibration of the model soils and geogrid components separately and then in a composite arrangement is crucial. The calibrations are conducted by comparing the results of laboratory testing of real material with the identical arrangement using the DEM model. Close comparison of results is necessary to confirm that the model is an accurate representation.

2. SOIL MODELLING IN PFC_{3D}

Special attention has been given to the simulation of the granular soil. In our experience a simulation of an existing soil based on its geomechanical physical properties alone is inadequate. It is necessary to recognize the crucial role of the fines, the angularity and the distribution of particle shapes. These must be correctly represented in the model. Specially prepared granular soils have been selected and analyzed in order to model these soils correctly (Stahl and Konietzky 2011).

If grain shape, grain size and relative density are carefully analyzed and considered, a relatively simple constitutive relation for the interaction of the grains (linear contact model) can be established. Just three constant values for shear stiffness, normal stiffness and friction coefficient are sufficient to simulate the mechanical behavior in terms of stress and deformation under quite different loading conditions (e.g. soil pouring, triaxial test, shear test (Stahl and Konietzky 2011)) and initial relative densities ID (ID025 = loose, ID075 = dense compactness).

The selected soils (Figure 1) are granular with approximately 98 % quartz, a grain density of 2.60 g/cm3 and a sphericity index of SI15 (rounded grains).

With respect to numerical constraints (i.e. calculation time), the following two calibrated grain-size distributions [16] have been selected to be used within this study: 12.5-16 mm and 5-32 mm.

Figure 1. Samples according to the grain-size distributions 12.5-16mm and 5-32mm, example of clump shape (right) [16]

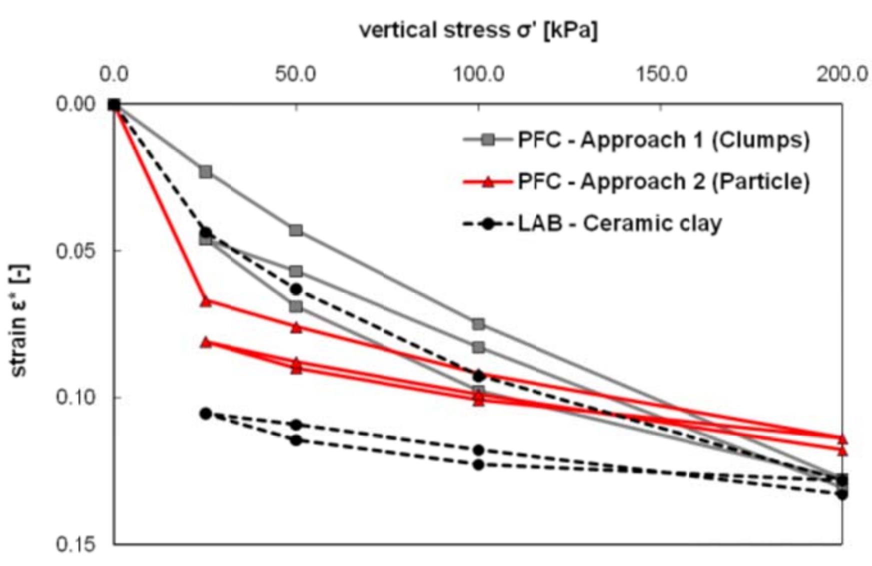

Figure 2. Results of the Oedometer test for the clay

The next stage is to create a realistic 'soft' clay soil layer underneath the geogrid-granular soil layer composite. The plastic behavior of the clay layer can be realistically modelled with separate spheres and allowing larger displacements (Approach 2 in Figure 2). Because of the computer calculation time the size of the spheres cannot be too small. During the calibration process the optimum size has been selected to be 11 mm. The rate of displacement of the spheres will be influenced by the selected porosity and by the layer thickness. For the 40mm thick layer of soft clay the porosity is 0.460.

The numerical calculation results (Figure. 2) show close comparison of the model to the stress-strain behavior measured in the laboratory using the Oedometer and a very satisfactory reproduction of the stiffness in the unloading and reloading cycles.

3. GEOGRID MODELLING IN PFC^{3D}

The first geogrid structure to be modelled was a stiff biaxial geogrid. This was later followed by the hexagonal geogrid with triangular apertures. The geogrid is modelled by strings of overlapping spherical particles of varying size, which accurately describe the geometrical aspects (Stahl 2011 & Stahl et al. 2013).
A parallel bond logic is used to bond the geogrid particles together at each contact point. The parallel bond approximates the physical behavior of a cement-like substance joining two bonded particles. These bonds establish an elastic interaction between particles that act in parallel with any other contact model at the contact.

Both types of geogrid have been submitted to a severe process of calibration where the physical properties of the model have been set and checked. This process included single rib tensile testing; full-width tensile testing (in accordance to ISO 10319) and aperture stability testing (Kinney 2000). In both cases the calibration of the model gave an excellent correlation with the laboratory testing of original products.

4. PULL-OUT TESTS

In order to calibrate the interaction behavior of a geogrid stabilized system, numerical pull-out tests based on the developed soil and geogrid model have been performed and validated in conjunction with experimental analysis using the ‘‘Geosynthetics-Soil-Testing-device’’ described by Aydogmus (2006) (Figure 3). For practical reasons the pull-out test was only performed with one geogrid type and the biaxial grid was selected. The calibration process is to determine a consistent set of micro-parameters for the contacts between clumps and geogrid particles to reproduce the real intensity of anchorage in terms of pull-out resistance. For this purpose, the calibration result obtained from biaxial geogrid testing is applicable to both forms of geogrid structure under consideration.

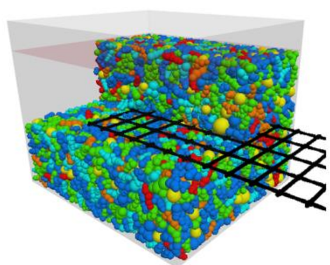

Figure 3. Pull-out test set-up in PFC^{3D}

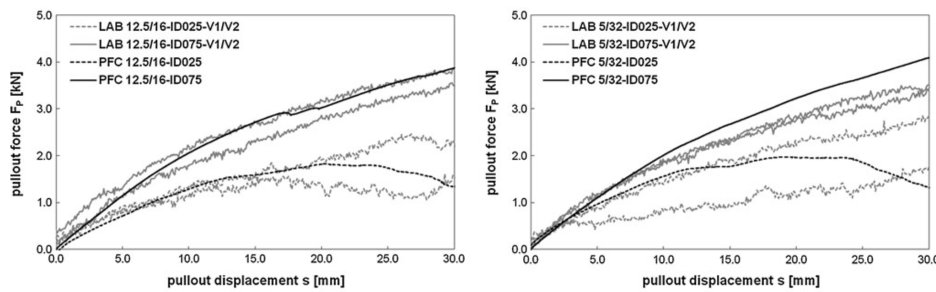

Figure 4. Pull-out force-displacement behavior versus corresponding Lab results

The results of the numerical pull-out simulations (Stahl et al. 2013) in terms of pull-out force–displacement behavior show qualitative agreement with experimental data in conjunction with various test conditions (Figure. 4).

5. PLATE LOADING

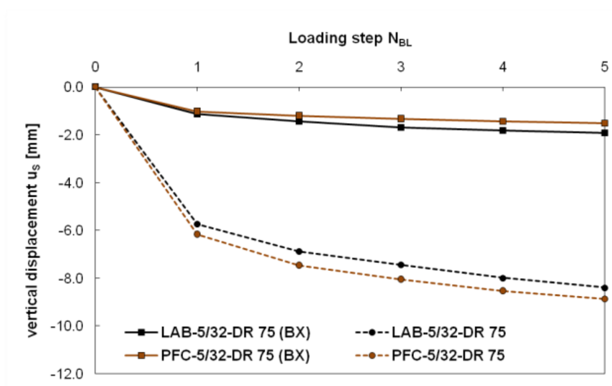

Figure 5. Plate-load test comparisons for stabilised and non-stabilised

In order to double check the interaction behavior of a geogrid-stabilized sub-base, numerical plate-loading tests based on the developed soil and geogrid model have been performed and in validated in conjunction with laboratory plate load tests using a specially developed box (Jas et al 2015). Earlier research trials had shown that even the smallest differences, such as shape of stones, quantity of fines, density, box size, surcharges, etc. could cause differences in behavior.

The results of both the pull-out and the plate-loading (Figure. 5) gave such a good correlation between the experiments and the numerical calculation that the model and the installation procedure have been fully validated and can be confidently used for further investigations.

As the TX hexagonal geogrids were not yet available during this calibration process a decision was needed whether to recalibrate for the hexagonal geogrid and soil in the same manner. As the calibrations of the physical properties of the hexagonal geogrid were equally successful as for the biaxial geogrid it decided that there was no need to repeat the work.

6. WHEEL LOAD SIMULATION

6.1 Set up and installation

In order to analyze the fundamental effects of geogrid-stabilized systems on a micro-level, a wheel load simulation based on the modelled soils and geogrids with fully calibrated micromechanical properties has been developed and set-up (Figure. 6). A soft subgrade layer modelling approach is used to intensify the effective mechanisms.

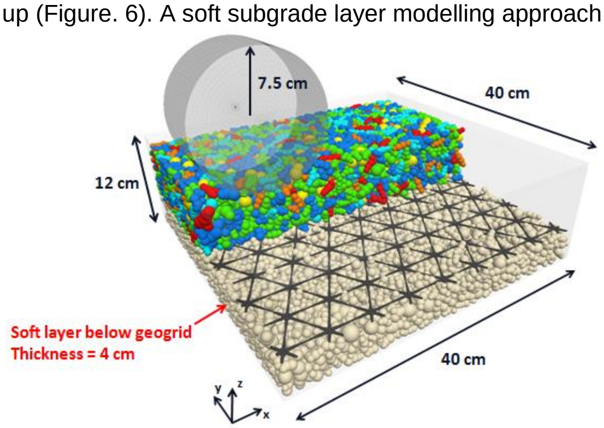

Figure 6. Wheel load test set-up

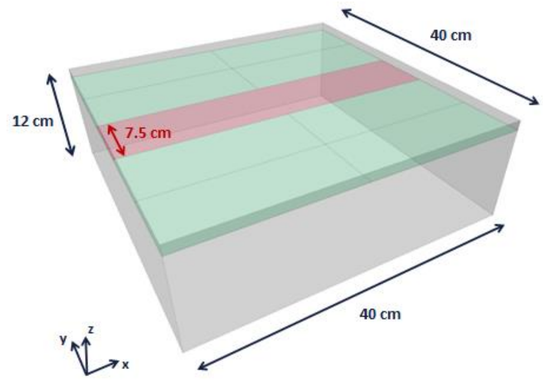

Figure 7. Box geometry and subdivision of top wall

The test set-up of the wheel load simulations in PFC^{3D} can be described as follows: At first a square testing box was created. The top wall was subdivided into nine walls. One wall was generated along the wheel passage (width=7.5 cm) and the other eight walls ensure a consistent distribution of contact forces within the test specimen. In consideration of boundary influences, resulting clump particle numbers and calculation time, a box geometry of 40 x 40 x 12 cm (L x W x H) was selected (Figure. 7).

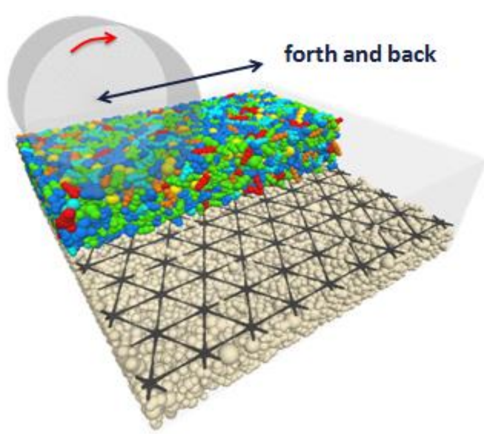

Figure 8. Wheel load test procedure

The soil was numerically generated consisting of a 4cm thick soft subgrade layer at the bottom of the box and an overlying 8cm thick base layer (calibrated granular material 5-32mm). The geogrid was installed between the base and the subgrade layer. An important aspect in this context was to use a special installation procedure to guarantee effective interlock between the geogrid and soil clumps.

After the installation of the soil and the geogrid, a consolidation phase was performed in which a vertical stress of 5 kPa was applied to the whole specimen to create a uniform contact distribution between the particles. In the next step, a wheel (cylinder with a radius and width of 7.5 cm) was created at the left side of the box (starting point). After the generation of the wheel a first load of 50N was applied at the contact zone of wheel and clumps.

The wheel load tests were performed by rolling the wheel along the passage back and forth with a constant velocity of 0.5 m/s (Figure. 8). A final wheel load value of 500kN (applied at the contact zone of wheel and clumps) was used based on the assumptions for a real vehicle wheel (uniform constant pressure of 75 kPa). During the test a constant vertical stress of 5 kPa was applied on the top walls.

The whole simulation requires over 100,000 spheres of which interactions need to be calculated (iteratively) at every step. A calculation of 10 runs with the 5-32 soil can take a few months even on the fastest PC single processor!

6.2 Results

Two cases with geogrid are presented: one with a biaxial geogrid (SS) and one with a TX hexagonal geogrid grid (TX) of equal weight. The results can be split in three parts:

1. The deformation of the surface gives a very good impression of the representation of the simulation with regard to real trafficking;
2. The actual (accumulative) displacement of the particles during the passage of the wheel to the 9^{th} run shows how the particles react due to the influence of the stabilizing geogrid, and
3. The actual physical behavior of the geogrid shows how the geogrid exercises the stabilizing effect.

6.2.1 Surface deformation

Before the results are discussed it is appropriate to say a few words about the particle interaction. In the computer simulation one gives certain properties to the soil (for instance friction between the soil particles). This does not change during the simulation, no matter what kind of action (loads, vibrations, wheel passes) will be exercised on the model. This is one notable difference between the experiment and the model. As such while the comparative data are very valuable, absolute data need to be treated with care.

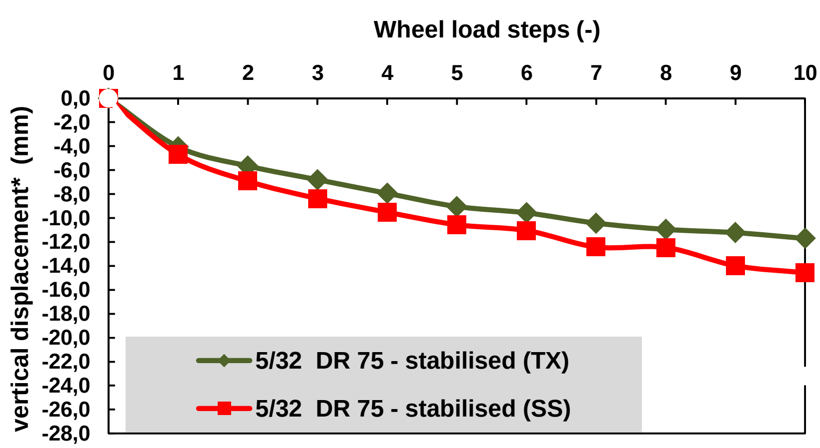

Figure 9**:** Surface deformation of the model

These results (Figure 9) show that the computer simulation actually gives a very realistic representation of the surface deformation. Although the surface deformation seems to show equal performance, the TX geogrid actually needs 50% more passes to reach the same deformation.

However, it must be emphasized that these are only the very first runs over a granular sub-base and they do not indicate the efficiency of the grids as such.

6.2.2 Displacements of soil particles

The figures below (Figures 10-12) are snapshots of a cross-section showing the individual particles and indicating with colors the magnitude of their displacements. The displacements of the granular particles in line with the wheel path show a clear reduction of the subgrade deformation when stabilized with a geogrid. Obviously, the maximum displacements are directly under the wheel, and reduce downwards. The stabilizing grids show a clear borderline of the displacement, protecting the weaker clay efficiently. Already a difference between a biaxial grid and TX grid is clearly visible.

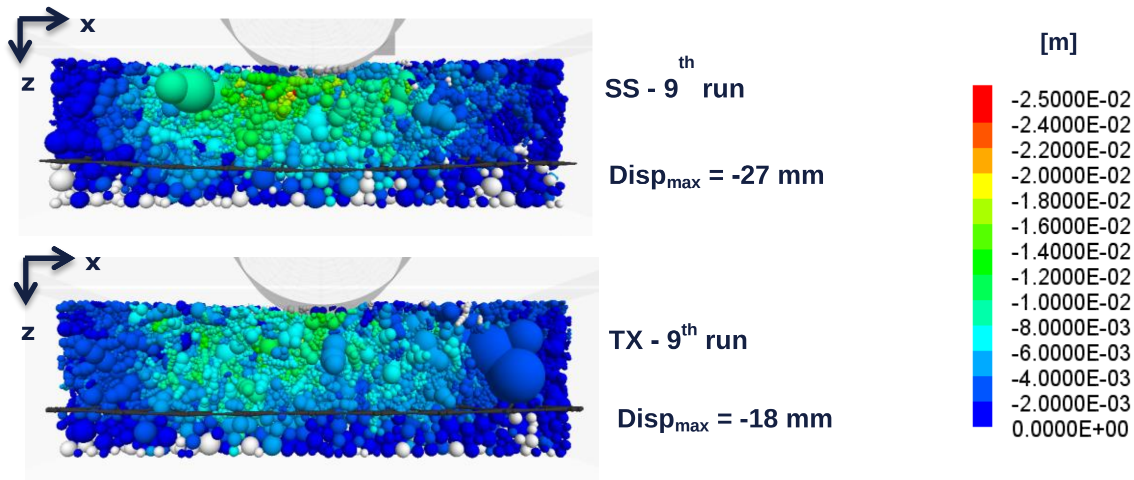

Figure 10. Cumulative X-Z displacements (in line with wheel path) of the granular particles after the 9th run.

The displacements perpendicular to the wheel path (Figure 11) give a good idea of stabilizing effects of the geogrids. Where the mode stabilized with the SS grid shows a relatively wide spread of the displacements, the model stabilized with the TX geogrid shows a much narrower band of displacements. The confining effect of the geogrids prevents a lateral displacement of the granular particles.

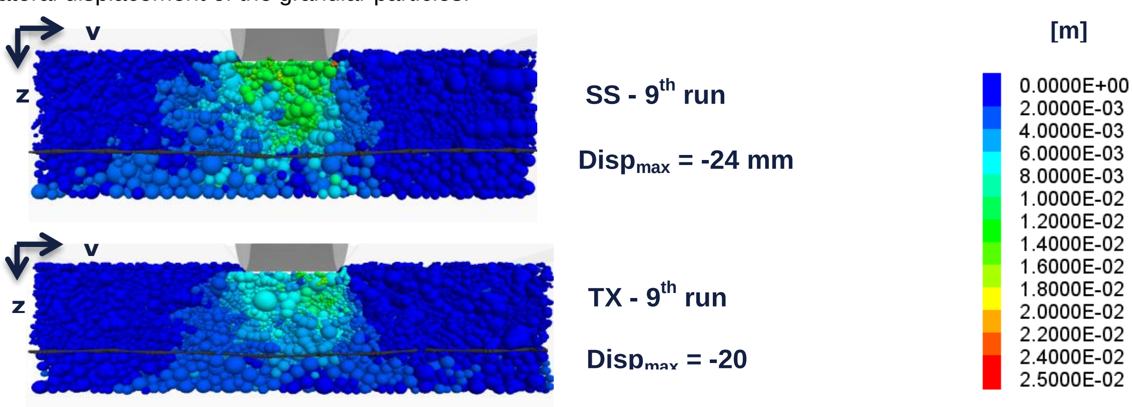

Figure 11. Cumulative Y-Z displacements (across the wheel path) of the granular particles after the 9th run

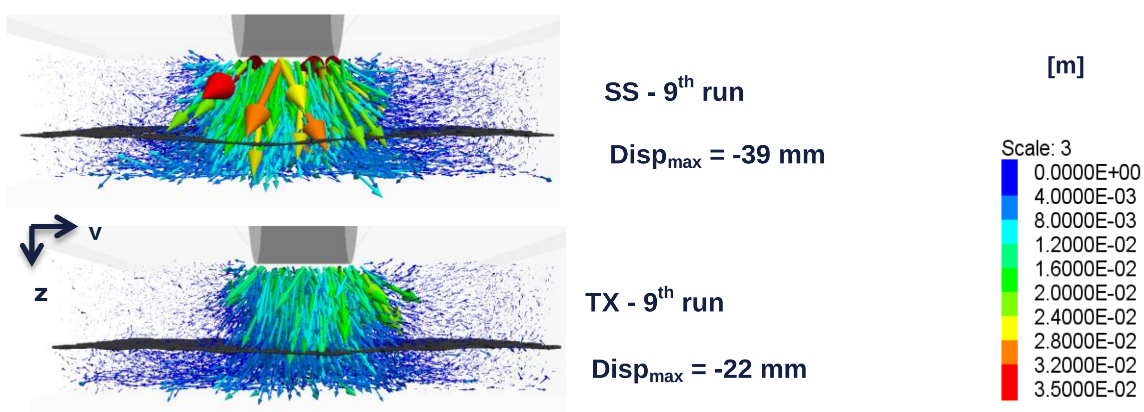

Figure 12. Total cumulative displacements of the granular particles after the 9th run.

The total displacements of the particles of the granular sub-base show similar results. All in all, a geogrid will reduce the displacement of the granular particles to 39 mm (SS) and to 22mm (TX). This will reduce the average rut depth in the wheel path from 22 mm to 14 mm (SS) and 11 mm (TX). Please note the significant differences between the geogrids, however small in absolute size.

6.2.3 Physical behavior of the geogrid(s)

The displacements of the granular particles confirm what most leading technologists and experts have presumed for years. However, for the very first time we have the possibility to look at the physical behavior of the geogrids under a sub-base when loaded by a passing wheel.

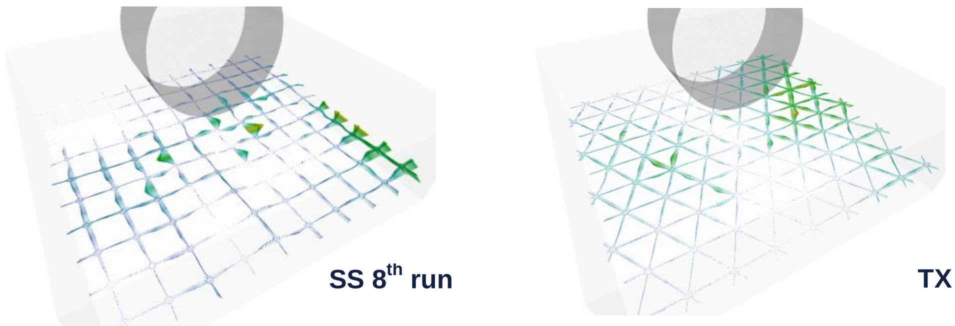

Figure 13**.** In plane displacement measured against the zero position, with $Disp_{max}$ = 0.5 mm (SS) and 0.23 mm (TX)

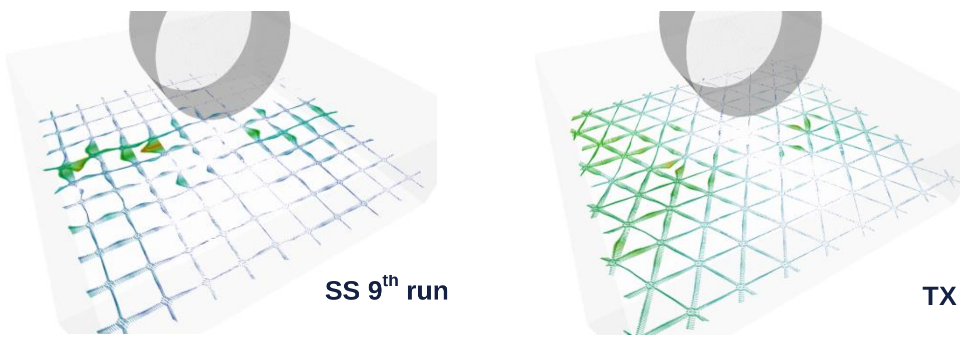

Figure 14. In plane displacement measured against the zero position, with $Disp_{max}$ = 0.52 mm (SS) and 0.24 mm (TX)

The reaction of the geogrids to the loads from the granular particles is shown by their deformations in the plane. Clearly one can see the reaction of the geogrids to the movements of the stones in Figure 13 and Figure 14. The movements are accumulated and very small. The images are snapshots taken at a certain time and can be very misleading. They could show some “extreme or particular” cases and indicate that one needs to be very careful not to read too much into them.

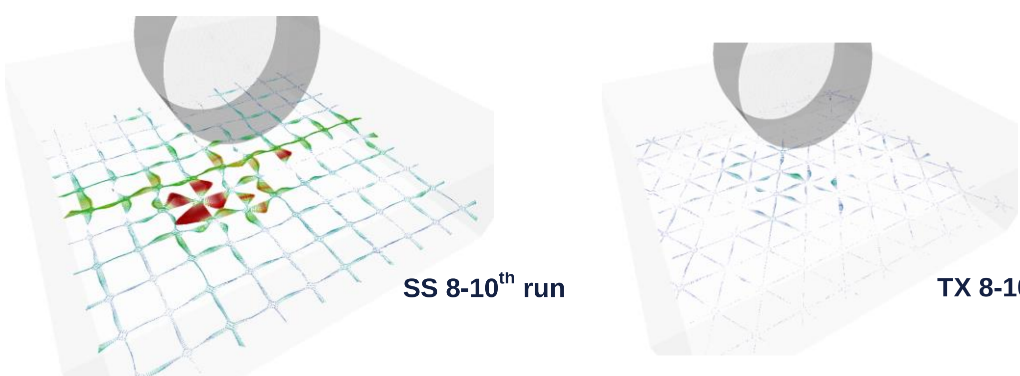

Figure 15. In plane displacement for 8th to 10th run, SS and TX grid. ($Disp_{max}$ = 0.39 mm respectively 0.20 mm)

It might be better to look at the displacements in the plane between two successive runs (Figure 15). The biaxial geogrid rotates around the node! The forces exerted by the stones of the sub-base on the ribs of the grid, will bend the ribs and will be transferred to the adjacent ribs of the node. Clearly the stiffness and strength of the node will have to be an important characteristic.

The TX grid hardly twists - the individual ribs do bend a little bit, but there is very little movement of the junctions. It seems that the grid is at rest. Please note that the largest movement in these graphs (Figure 15) is only 0.4 mm for the biaxial grid and 0.2mm for the TX grid!

In order to provide a visualisation of the tensile behaviour of the geogrid, the stresses between the spheres have been transformed into forces, using the diameter of that sphere. In this way the different diameters of the spheres have been eliminated (Figures 16 and 17).

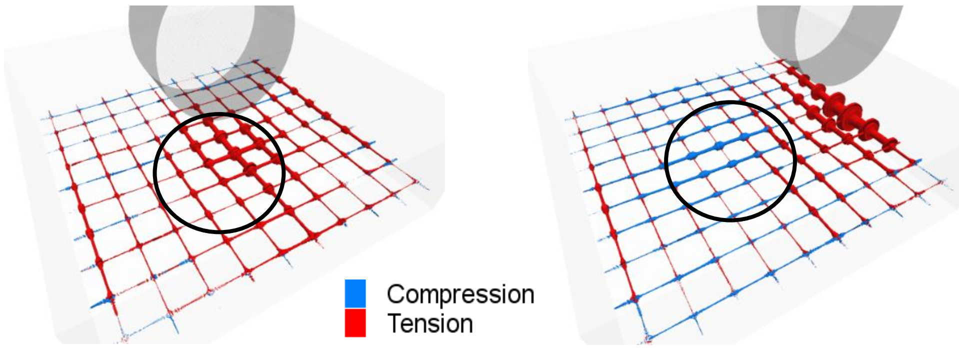

Figure 16. The forces in the ribs of SS at the 9th run (from 19 to -10 N per rib).

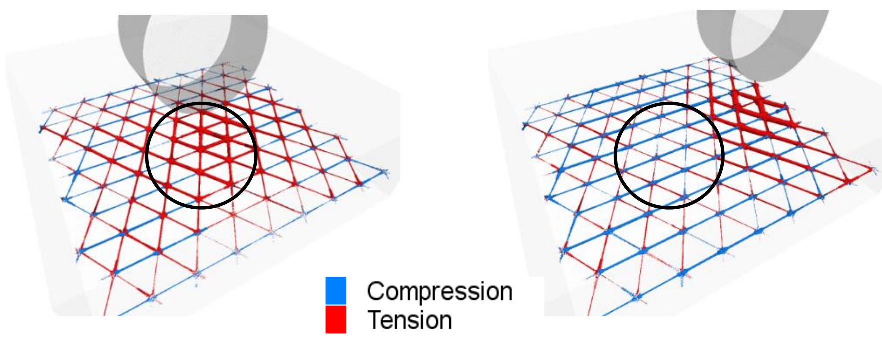

Figure 17. The forces in the ribs of TX at the 9th run (from 10 to -7 N per rib).

There are four points that need to be noted:

1. The grids are not only under tension: they are under compression as well. This is quite logical, but probably never well understood. One needs to appreciate that the geogrid installed in the pavement of a road is in principle at rest! The only loads exercised are the weights of the surcharge (the various layers of the pavement). It is only when the road is being trafficked that the granular particles will transfer loads on to the grids. See also the EOTA definition of stabilization (EOTA TR 041 (2012). It is clear that both grids stabilize a granular layer over a weak sub-grade!

2. The magnitude of the forces and strains in the grids (both in tensile and in compression) is very small. They are less than 0.7 kN/m' and for TX grids even less than 0.3 kN/m'. The strains are on the order of 0.5%! This is a very small proportion of the total tensile capacity of the geogrids and it proves again: Ultimate tensile strength is NOT relevant for sub-base stabilization applications.

3. The forces in the grids (Figure 16) show that the biaxial grids transfer the tensile load across the wheel path anchoring themselves in the adjacent areas that are not loaded and the compressive load in the line of the wheel path. These areas are not very wide, as the loads are relatively small. But the mechanism is one of tension in the ribs and pressure in the aggregate.

4. The TX grids transfer the forces from the granular particles in the near circular shape of the concentric hexagons formed in the grid (See Figure 17). Six triangles of the geogrid form a hexagon. But there is another hexagon concentric around the inner one, and this geometry continues outward. When these hexagons are under tension they confine the granular particles due to the tension-ring effect that we know from domes, etc. Observations of the video of the model created from the wheel passing from one end to the other shows that when the wheel passes the hexagons that are under tension will move with the wheel. Actually, the active tension-rings will transfer along the geogrid, we may refer to this as a Sequential Overlapping Tension Ring effect.

7. CONCLUSIONS

The main conclusion is that it is possible to use Itasca's Particle Flow Code PFC^{3D} to simulate soils, geogrids and the interaction between them creating very credible results. Although the simulation of a wheel passing a stabilized granular sub-base on a weak sub-grade has certain limitations, it creates a very credible insight in the behavior of the geogrid.

Another main conclusion is that both types of geogrid have a stabilizing effect on granular layers under a wheel load.

The actual forces and strains in the grids (both SS and TX) during the passage of a wheel are very low (less than 1kN/m' and around 0.5%). Actually the grids are under compression as well!

When a soil particle exercises a force onto a biaxial grid (perpendicular to a rib), the adjacent junction(s) will rotate. Depending on the stiffness of the junction, that moment will be transferred to the other ribs and junctions. The force will then be transferred through the ribs and transferred back to the soil by anchoring outside the loaded area. Main characteristics will have to be torsion stability (Webster of the USACE) and stiffness at very low strain.

The hexagons of the grid confine the granular particles, creating a (near circular) tension in the ribs of the hexagons (tension-rings). Such a hexagon will be placed under tension when the wheel arrives and the ribs go into compression after the wheel has passed. Actually the active tensioned hexagon will transfer from one to the other, moving with the wheel load (Sequential Overlapping Tension Rings). Consequently, a junction will experience different stresses and strains from the six ribs (both in tension and in compression). In order to allow such a Tension Ring effect with very small deformations in the geogrid, the stiffness of the ribs around the junction must be equal in all directions! Therefore, the main characteristics will have to be near uniform stiffness at very low strain in all directions.

ACKNOWLEDGEMENTS

The authors wish to acknowledge the company Tensar International Limited for providing the geogrids needed to perform the laboratory tests. Furthermore, the authors would like to thank Prof. Dr. Frank Otto (TFH Georg Agricola Bochum) and Dr. Florian Bussert for technical discussions. Laboratory tests were conducted at the Geotechnical Institute, TU Bergakademie Freiberg, Germany.

REFERENCES

ASTM D 6637 (2001) Standard test method for determining tensile properties of geogrids by the single or multi-rib tensile method (SRTT)

Aydogmus T (2006) Beitrag zum Interaktionsverhalten von Geokunststoffen und Lockergestein. Veröffentlichung des Instituts für Geotechnik der TU Bergakademie Freiberg (Heft 2006-6), Hrsg. Klapperich & Konietzky

Chen C, McDowell GR, Thom NH (2012) Discrete element modelling of cyclic loads of geogrid-reinforced ballast under confined and unconfined conditions. Geotextiles & Geomembranes 35:76–86

EOTA Technical report TR 041: Non-reinforcing hexagonal geogrid for the stabilization of unbound granular layers by way of interlock with the aggregate, October 2012

Fellerec J-F, McDowell GR (2010) A method to model realistic particle shape and inertia in DEM. Granular Matter, vol 12. Springer, Berlin, pp 459–467

GRI-GG2 (2005) Standard test method for ''Individual Geogrid Junction Strength'' (IGJS). Geosynthetic Research Institute Folsom, USA

Itasca Consulting Group Inc (2008) PFC3D Version 4.0—Manuals 1-6. Minneapolis, USA

Jas H, Stahl M, Konietzky H, te Kamp L, Oliver T (2015) Discrete Element simulation of geogrid stabilized sub-base: Modelling and calibration and plate load simulation under special consideration of important boundary conditions, 6th Symposium on Deformation Characteristics on Geomaterials, Buenos Aires, November 2015, To be published.

Kinney TC (2000) Standard test method for determining the ‘‘Aperture Stability Modulus’’ of a Geogrid (ASMT). Shannon and Wilson Inc, Seattle, USA

Konietzky H, te Kamp L, Groeger T, Jenner C (2004) Use of DEM to model the interlocking effect of geogrids under static and cyclic loading. In: Shimizu, Hart, Cundall (eds) Numerical modeling in micromechanics via particle methods. Balkema, Leiden, Netherlands, pp 3–11

McDowell GR, Harireche O, Konietzky H, Brown SF, Thom NH (2006) Discrete element modelling of geogrid-reinforced aggregates. Proceedings of the ICE—geotechnical engineering, vol 159(1), ICE Publishing, London, UK, pp 35–48

Qian Y, Tutumluer E, Huang H (2011) A validated discrete element approach for studying geogrid-aggregate reinforcement mechanisms. In: Han, Alzamora (eds) Proceedings of the ASCE Geo-Institute Geo-Frontiers conference on advances in geotechnical engineering, 13.-16. March, Geotechnical Special Publication 211, Dallas, Texas, USA

Stahl M (2011) Interaktion Geogitter-Boden: Numerische Simulation und experimentelle Analyse. Technische Universität Bergakademie Freiberg, Heft 2011-5

Stahl M, Konietzky H (2011) Discrete element simulation of ballast and gravel under special consideration of grain-shape, grain-size and relative density. Granular Matter vol 13. Springer, Berlin, pp. 417–428

Stahl M, Konietzky H, te Kamp L, Jas H (2013) Discrete element simulation of geogrid-stabilized soil, Acta Geotechnica, Springer, DOI 10.1007/s 11440-013-0265-0

Ziegler M, Heerten G, Ruiken A (2008) Progress in the understanding of geosynthetic/soil composite material behavior in geosynthetic reinforced earth structures. In: 1st Pan American geosynthetics conference and exhibition, 02.-05. March, Cancun, Mexico